Modelling adsorption interactions between vanadium incorporated on hydroxyapatite and the RR141 dye: Monte Carlo approach and DFT.

Fatima Zahra Chajri[1,2*], *Fatima Zahra Karmil*[3], *Nouhaila Benaissa*[2], *Meryem Bensemlali*[1], *Mohammed el idrissi*[4], *Meryeme Joudi*[1], *El Jouad Zouhair*[2], *Mohamed Monkade*[2], *Mina Bakasse*[1], and *Hamid Nasrellah*[1,5]

[1]Faculty of Sciences, Laboratory of Organic Bioorganic Chemistry and Environment, Chouaib Doukkali University, El Jadida, Morocco

[2] Faculty of Science, Physics of Condensed Matter Laboratory, Chouaib Doukkali University, El Jadida, Morocco

[3]*Laboratory of Physical Chemistry of Materials, Faculty of Sciences, University Chouaib Doukkali, El Jadida, Morocco.*

[4]Laboratory of Chemical Processes and Applied Materials, Polydisciplinary Faculty, Sultan Moulay Slimane University, Beni-Mellal, Morocco

[5]Higher School of Education and Training, Chouaib Doukkali University, El Jadida, Morocco

Abstract. The substitution of vanadium in hydroxyapatite (HAP) presents promising possibilities for advanced adsorption and electronic applications. This study focused on two key aspects of this material. Firstly, Monte Carlo calculations were conducted to examine the adsorption processes of the dye Reactive Red 141 (RR141) on the (001) surface of vanadium-incorporated nanohydroxyapatite NPs-HAP/VAP ($Ca_{10}(PO_4)_{6-x}(VO_4)_x(OH)_2$ with x ranging from 0 to 6). These findings suggest that the adsorption is spontaneous, and the energy increases as the vanadium content increases. This implies that pure HAP needs more energy to desorb RR141 than is needed to desorb its vanadium-containing counterpart. Another notable advantage of the presence of vanadium is its impact on the stability of the molecular structure, which is important in the tune of adsorption properties. Moreover, the electronic properties of NPs-HAP/VAP were predicted using Local Density Approximation (LDA) and Generalized Gradient Approximation (GGA) through the Density Functional Theory (DFT). The substitution related lattice changes were also studied. In the C-axis, GGA estimates an anisotropic expansion whereby the highest expansion is 13.27% at full phosphorus substitution, whereas LDA estimates an isotropic expansion whereby the highest expansion is 9.95%. The electronic property analysis reveals that the addition of vanadium into the NPs-HAP/VAP structure provides allowed states, mostly built on the d electrons of vanadium, interacting with the O-2p electrons in the band gap, which accounts for the narrowing of the gap.

*Corresponding authors: chajri.f@ucd.ac.ma

1. Introduction

Hydroxyapatite (HA) is a natural mineral, which forms one of the major components of human bones and teeth. Its capacity to adsorb different molecules has attracted a lot of research attention [1–3]. This involves adsorption of ions, organic molecules, proteins, and drugs, and is applicable in many biomedical, industrial and environmental applications [4,5]. Thus, the insights into the adsorption mechanisms on the surface of this material are critical to maximizing the applications.

Among them, one issue is textile dye, RR141, which is very popular in industry. Nevertheless, it may be present in the industrial effluent that may pollute water and be hazardous to the environment and human well-being [6,7]. Consequently, it is important to develop materials that could be used to adsorb such dyes in order to treat waste water and pollute the environment [8–12].

One of the most significant problems of the adsorption process is the development of adsorbents with high adsorption capacity and quick reactivity in the context of being cost-efficient and environmental-friendly[13,14]. Although the cost-effective adsorbents have economic advantages, they tend to have decreased adsorption capabilities. In this regard, hydroxyapatite vanadate nanoparticles (NPs-HAP/VAP) based on waste products of the phosphate industry, including phosphogypsum and vanadium pentoxide have been developed to solve this problem [15,16].

The adsorption of RR141 dye on NPs-HAP/VAP surface has been studied previously in that study [17]. The findings depicted an adsorption capacity of 50mg/g and total removal of the dye. The process of elimination was based on the pseudo-second order and SIPS model. The thermodynamic calculations were showing spontaneous adsorption which implied that positive changes in the entropy are amplifying the physical nature of the process. The characteristics of adsorption of RR141 were determined and quantified in this experiment. Nevertheless, to have a better understanding of the mechanisms of this interaction, we should use the theoretical approaches.

Monte Carlo simulations were performed as a part of this research to investigate the adsorption of RR141 on the (001) surface of the material $Ca_{10}(VO_4)_x(PO_4)_{(6-x)}(OH)_2$[18–23]. Adsorption Locator tool was used to make these calculations. The main aim of the study was to consider the possible adsorption of RR141 using the hydroxyapatite NPs-HAP/VAP nano-vanadates and determine their most stable forms and complexes. Total energy, adsorption energy and Van der Waals energy parameters were considered. This methodology seeks to give an enhanced insight into the adsorption processes of $Ca_{10}(VO_4)_x(PO_4)_{(6-x)}(OH)_2$ (for x=0,1,2,3,4,5, and 6) (where x=0,1,2,3,4,5 and 6) with respect to the RR141 pollutant, and determine preferential adsorption sites. This study has a great research implication in the removal of dye and purification of water.

2. Simulations Monte Carlo

There are many applications of the Monte Carlo method in simulation especially in the case of global minimization of a system. The technique is based on random iterations and relaxations. A random motion initiates the process. First, the energy of the current system is calculated. Next, one of the atoms in the system is randomly shifted, and the energy of this new configuration is computed. The energies of the initial and new configurations are then compared.

If the energy of the new configuration is lower, it is accepted, meaning the new configuration replaces the initial one. However, if the energy of the new configuration is higher, the Boltzmann probability is calculated to determine whether the new state should still be accepted [24] :

$$e^{-\frac{\Delta E}{K_B T}} \qquad (1)$$

Where ΔE is the energy difference, KB is Boltzmann's constant, and T is the temperature setting. A random number m is generated within the range [0, 1]. If m > p, the initial configurations are retained, with the hope of escaping a local minimum to reach the global minimum by overcoming a certain energy barrier. This process is repeated over a given period. In this manner, a Markov chain is generated with N configurations. The system's temperature is adjusted either linearly or exponentially, and the previous steps are reiterated using the configurations from the Markov chain. When the temperature is reduced systematically until a given criterion is reached, a global minimum may be reached. with the Monte Carlo (MC) technique.

Nevertheless, the MC approach has certain weaknesses: calculation time grows very fast with the size of the system; it may require too much time to discover the global minimum; and the initial parameter settings should be as the size of the system increases. meticulously planned, since they might have a considerable impact on the end outcomes.

3. Results and discussion

3.1. Monte Carlo simulation of Reagent Red 141 (RR141)

Adsorption of the RR141 dye onto solid adsorbent is a good and eco-friendly process of eliminating dyes in polluted water sources. It is important to understand the adsorption behaviour of the RR141 dye molecules on the different

adsorbents to optimize the adsorption processes and in the design of a good dye removal system. This paper examined the property of adsorption behaviour of the RR141 dye via Monte Carlo simulations, which was developed in the Adsorption Locator tool. This study was to explain the underlying mechanics of the adsorption process by just applying Monte Carlo simulations. The lessons learned in this study could be used in the development of cost-effective and sustainable measures on how to eliminate RR141 dye and other contaminants in the wastewater streams.

The adsorption energy of the lowest-energy configuration obtained due to the interaction of the RR141 molecule with the (001) surface of various vanadate/hydroxyapatite structures which are denoted as $Ca_{10(}VO_4)_x(PO_4)_{(6-x)}$ $(OH)_2$ with the vanadate ratios varied was determined using Monte Carlo (MC) simulations. The methodology that was used to construct the adsorbent / substrate system was the Metropolis Monte Carlo simulation approach combined with the Adsorption Locator tool. The simulations were conducted using a plate thickness of 5 A and a void of 30 A in the C-axis direction and periodic boundary conditions were used to model a representative slice of the interface avoiding arbitrary boundary effects. The various systems ($Ca_{10}(VO_4)_x(PO_4)_{(6-x)}(OH)_2$/RR141) were optimized using the COMPASS (Condensed Phase Optimized Molecular Potentials in the study of Atomistic Simulations) force field during the process of the simulation.

This computational analysis will determine low-energy adsorption sites to determine the selective adsorption of inhibitors molecules onto the NPs-HAP/VAP surface. In order to accomplish this, the NPs-HAP/VAP (0 0 1) surface configurations were sampled in a canonical set, in which individual RR141 molecules were taken into consideration. Through optimization of the system, different energies were obtained such as total energy, Van der Waals energy, electrostatic energy and intermolecular energy as illustrated in **Fig. 1**. This discussion gives a clear insight into the interactions of the surface and the molecule, RR141.

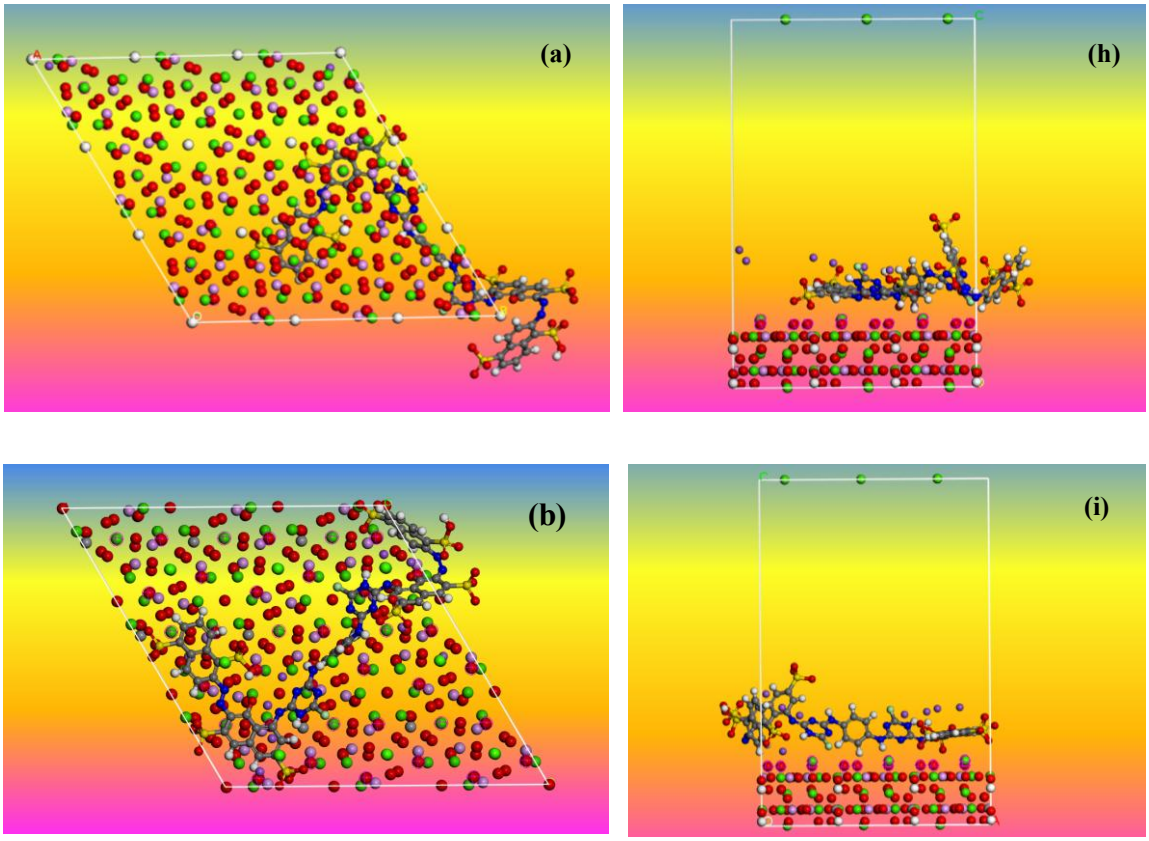

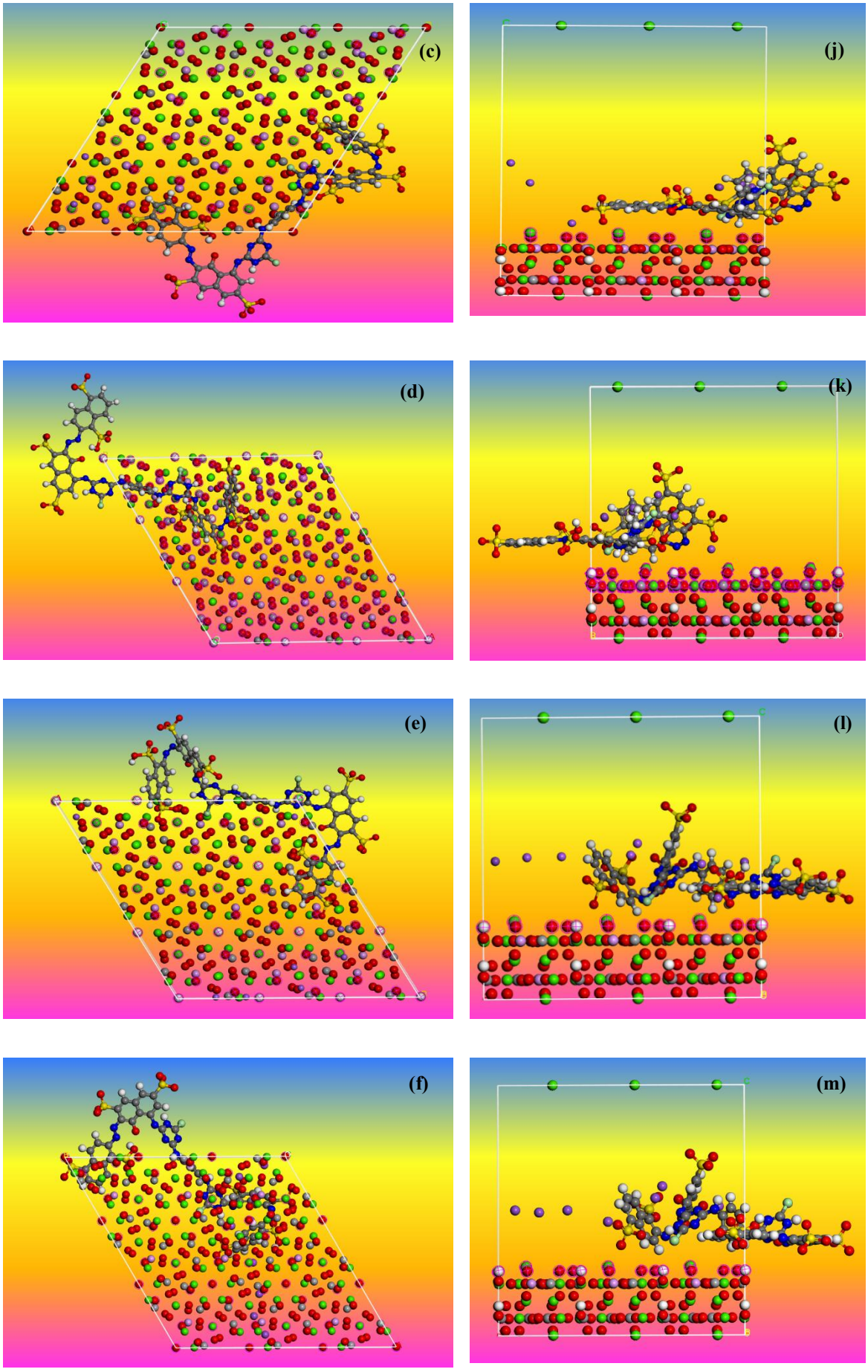
(c)
(j)
(d)
(k)
(e)
(l)
(f)
(m)

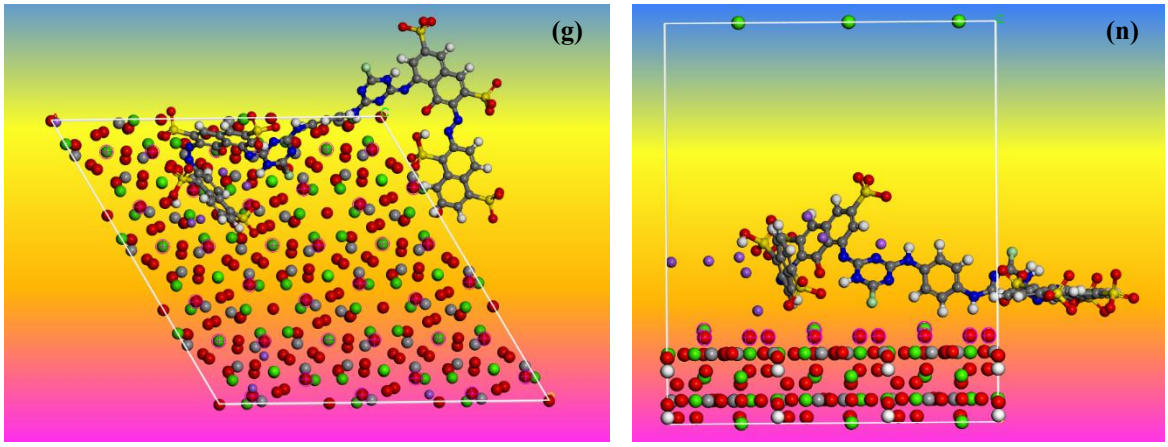

Fig. 1: (a)-(g) Top view and (h)-(n) side view of the different structures of $Ca_{10}(VO_4)_x(PO_4)_{(6-x)}(OH)_2$ for x = 0, 1, 2, 3, 4, 5 and 6, respectively.

Fig. 1 illustrates the various adsorption centers of the RR141 molecule within the structures under consideration. In this study, the energy of the substrate is set to zero. The adsorption energy is defined as the total of the adsorption energy, the rigid adsorption energy (R.A.E.), and the deformation energy for the components of the adsorbate. The rigid adsorption energy represents the energy measured in kcal/mol, released (or required) when the unexpanded RR141 molecule, before the geometry optimization step, is adsorbed onto the (001) surface of the NPs-HAP/VAP.

Table 1: Results and descriptors of the lowest adsorption configurations for the $Ca_{10}(VO_4)_x(PO_4)_{(6-x)}(OH)_2$ (001) / (RR141) systems calculated by Monte Carlo simulation (all energy values in kcal/mol).

Structures	Total energy	Adsorption energy	Rigid adsorption energy	Deformation energy
$Ca_{10}V_6O_{24}(OH)_2$	871,1637	-41,0205	-43,5577	2,5372
$Ca_{10}P_1V_5O_{24}(OH)_2$	871,8498	-40,3343	-42,8607	2,5264
$Ca_{10}P_2V_4O_{24}(OH)_2$	864,6967	-47,4874	-50,6325	3,1451
$Ca_{10}P_3V_3O_{24}(OH)_2$	861,6437	-50,5405	-54,4924	3,9519
$Ca_{10}P_4V_2O_{24}(OH)_2$	861,9831	-50,201	-52,6511	2,4501
$Ca_{10}P_5V_1O_{24}(OH)_2$	859,2578	-52,9263	-57,5902	4,6639
$Ca_{10}P_6O_{24}(OH)_2$	858,0217	-54,1624	-57,9211	3,7586

The Deformation Energy represents the energy, measured in Kcal/mol, that is released when a molecule of the adsorbed component is released onto the surface of the NPs-HAP/VAP. **Table 1** displays these energies for the most stable configurations of the different $Ca_{10}(VO_4)_x(PO_4)_{(x-6)}(OH)_2$ structures, where x can take on values (x= 0, 1, 2, 3, 4, 5 and 6).

All the adsorption energies are negative, indicating that the adsorption of the RR141 dye by NPs-HAP/VAP is both possible and spontaneous. However, it's important to note that these energies increase with higher vanadium content in the basic crystalline structure, represented as $Ca_{10}P_6O_{24}(OH)_2$. The lowest adsorption energy is recorded for the $Ca_{10}P_6O_{24}(OH)_2$ material, at -54.162 kcal/mol. As the vanadium content increases (from x = 0 to x = 6), the energy rises progressively, reaching -41.0205 kcal/mol for the $Ca_{10}V_6O_{24}(OH)_2$material, which lacks phosphorus atoms.

Figures 1 (a) and **(h)** illustrate that the most favourable adsorption site for the RR141 molecule on the (001) surface of the $Ca_{10}P_6O_{24}(OH)_2$ material is the benzene ring, in which the molecule is adsorbed almost flat. In contrast, on the (001) surface of the $Ca_{10}V_6O_{24}(OH)_2$ material, the adsorption is tilted, resulting in a more deformed configuration of the molecule.

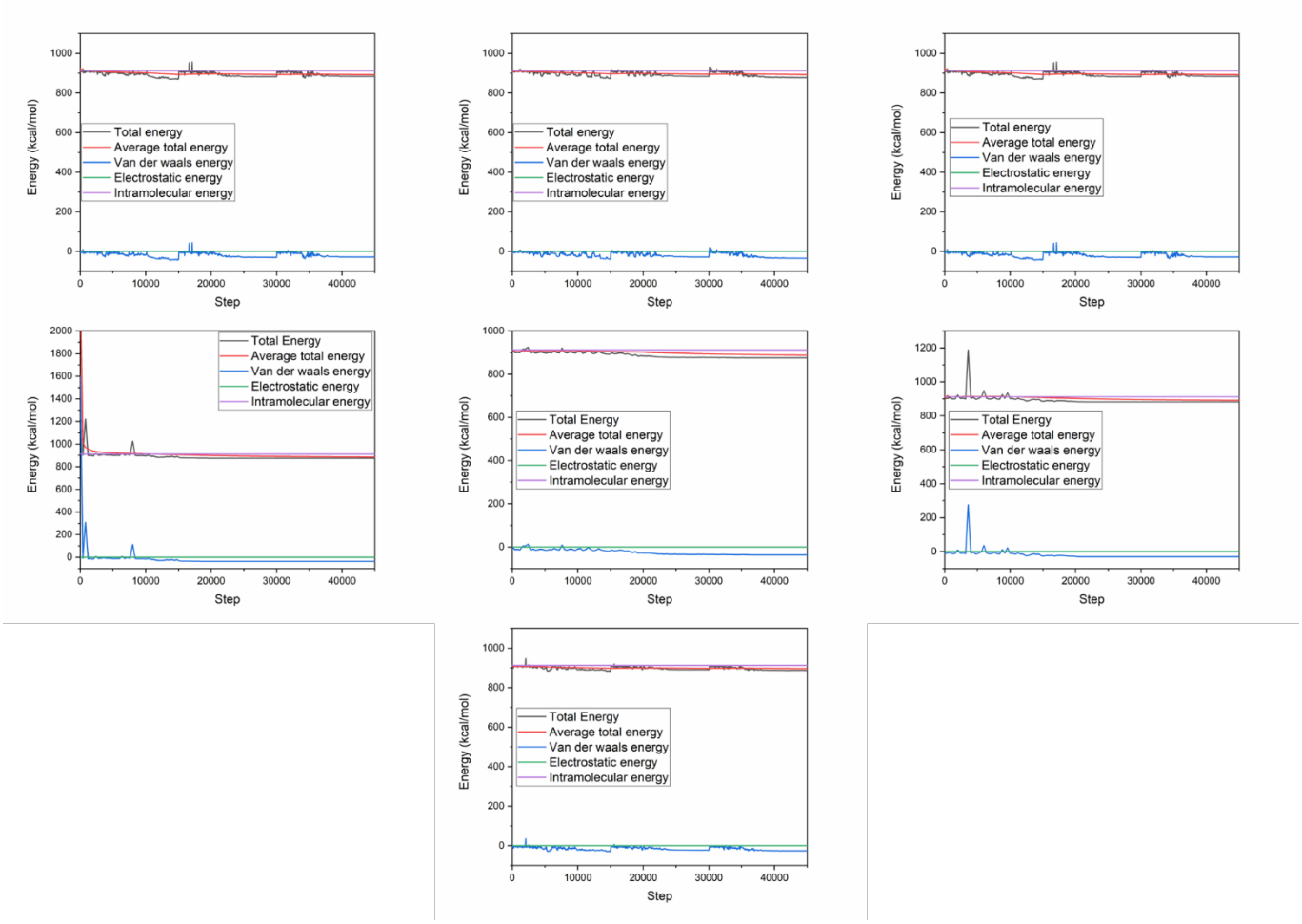

Fig. 2: Total energy distribution for the $Ca_{10}(VO_4)_x\ (PO_4)_{(6-x)}\ (OH)_2$ systems for x = 0, 1, 2, 3, 4, 5 and 6, respectively, using the Adsorption Locator model

3.2. DFT study of the electronic properties of hydroxyapatite vanadate

The CASTEP (Cambridge Serial Total Energy Package) code, which is based on density functional theory (DFT), was used to perform all the calculations presented in this work. For the exchange and correlation potential, two approximations were applied: the Generalized gradient approximation (GGA), implemented as the Perdew-Burke-Ernzerhof (PBE) approach, and the local density approximation (LDA).

A plane-wave basis set was used to solve the Kohn-Sham equations in the DFT implementation of the ultrasoft pseudopotential. Following the Monkhorst-Pack method for k-point sampling, the wave functions was extended with a plane wave energy cutoff of 340 eV and performed Brillouin zone integration using a 2 × 2 × 2 k-point lattice.

For optimizing the geometry, the convergence criteria were set with a maximum atomic displacement of 0.001 Å and an energy precision of 3.10×10^{-5} eV/atom. The equilibrium structural parameters were determined using the Broyden-Fletcher-Goldfarb-Shanno (BFGS) minimisation method.

Electronic properties such as band energies, total density of states (TDOS), partial density of states (PDOS) and chemical bonding conditions have been determined using electron density. It shows the energy scale, the likelihood of the presence of electrons and regions of minimal and maximum electron density. Also, the electron density is used to give information on sub-states including s, p, d and f states. The band structure provides data regarding the nature of the material such as whether the material contains a direct or an indirect band gap. Hydroxyapatite (HAP) crystal structure is of the P63/m space. In this structure, two oxygen atoms in the hydroxyl (OH) group occupy the fourth Wyckoff positions with each half occupancy. The geometry was optimized to attain a relaxed structure and calculations on the cellular properties of the relaxed structure were obtained and tabulated in **Table 2.**

Table 2: Lattice parameters in Angstroms calculated for the different structures.

Material	GGA		LDA	
	a	c	a	c
$Ca_{10}V_6O_{24}(OH)_2$	10,210	6,865	9,623	6,854
$Ca_{10}P_1V_5O_{24}(OH)_2$	10,149	6,847	9,545	6,834
$Ca_{10}P_2V_4O_{24}(OH)_2$	10,073	6,888	9,553	6,810
$Ca_{10}P_3V_3O_{24}(OH)_2$	9,869	6,881	9,399	6,792
$Ca_{10}P_4V_2O_{24}(OH)_2$	9,838	6,849	9,367	6,767
$Ca_{10}P_5V_1O_{24}(OH)_2$	9,744	6,881	9,293	6,761
$Ca_{10}P_6O_{24}(OH)_2$	9,593	6,878	9,249	6,748

Analyzing the results presented in **Table 2**, it can be observed that the lattice parameter (a), calculated using both the Local Density Approximation (LDA) and the Generalized Gradient Approximation (GGA) functionals, increases with higher vanadium content in hydroxyapatite. Specifically, the value of (a) rises from 9.593 Å for the $Ca_{10}P_6O_{24}(OH)_2$ structure to 10.210 Å for the $Ca_{10}V_6O_{24}(OH)_2$ structure, where all phosphorus atoms have been replaced by vanadium. . The two changes of the lattice parameter towards an increase in the (a) and (c) direction suggest that both are enlarged by the large size of the vanadium atoms relative to phosphorus.

It is important to note that the increase in lattice volume is predicted in only one direction according to the GGA calculations, which is evident from the fact that the (c) parameter fluctuates slightly around an average value of 6.869 Å. In contrast, calculations using the LDA approximation suggest that the expansion caused by the insertion of vanadium atoms into the original hydroxyapatite lattice occurs in all three spatial directions.

Table 3: Gap energies calculated experimentally and theoretically

	Energy Gap (eV)		
Structure	**Experimental** [17]	**GGA**	**LDA**
$Ca_{10}P_6O_{24}(OH)_2$	3,21	5,24	5,355
$Ca_{10}P_5V_1O_{24}(OH)_2$		3,738	3,856
$Ca_{10}P_4V_2O_{24}(OH)_2$		3,722	3,802
$Ca_{10}P_3V_3O_{24}(OH)_2$	3,16	3,702	3,868
$Ca_{10}P_2V_4O_{24}(OH)_2$		3,788	3,9
$Ca_{10}P_1V_5O_{24}(OH)_2$		3,689	3,835
$Ca_{10}V_6O_{24}(OH)_2$	3,04	3,754	3,857

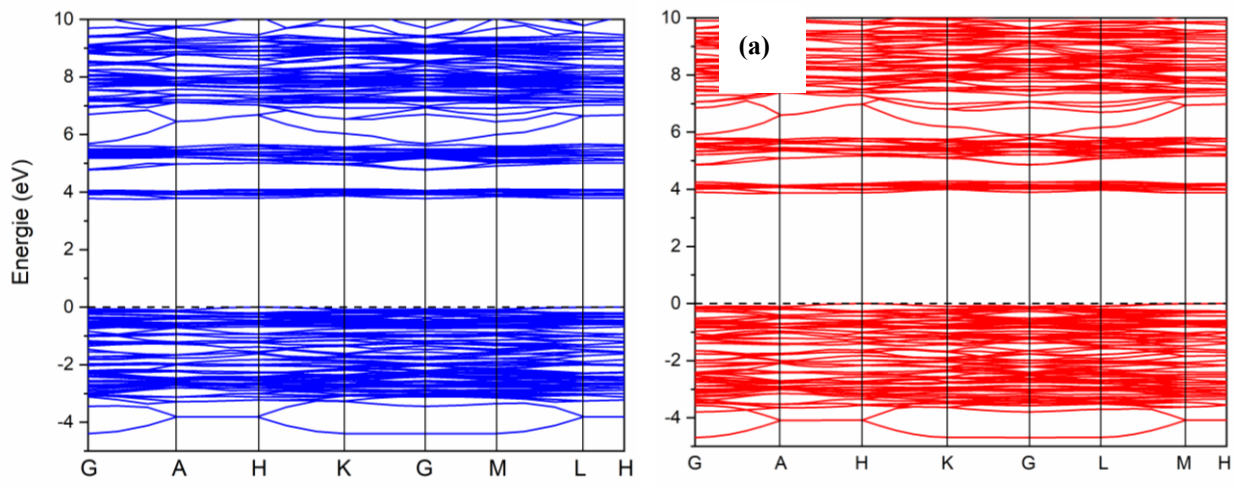

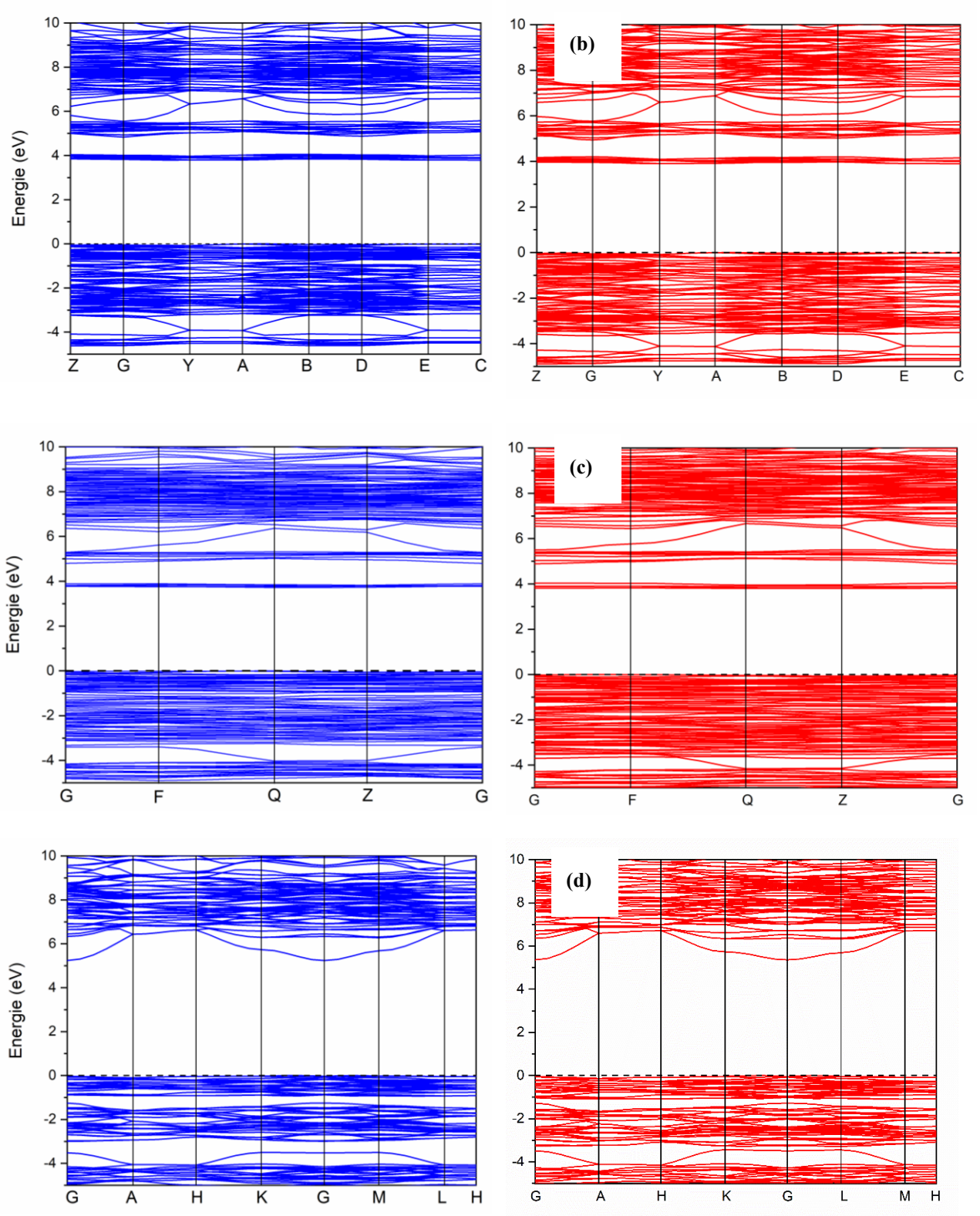

Fig. 3: (a)-(d) the band structures of the materials $Ca_{10}(PO_4)_x(VO_4)_{(6-x)}OH_2$ for x = 0, 2, 4 and 6 respectively. Calculated using the GGA approximation in blue and the LDA approximation in red.

The band structures calculated for various materials are illustrated in **Fig. 3** and **Table 3**. The results obtained using the Local Density Approximation (LDA) are shown in red, while those using the Generalized Gradient Approximation (GGA) are depicted in blue. In all the graphs, the energy origin is set at the Fermi level. The graphs indicate that the shapes of the band structures and the energy gaps are quite similar between the two approximations. Notably, hydroxyapatite retains its semiconducting nature even with the substitution of Vanadium atoms.

Hydroxyapatite $Ca_{10}(PO_4)_6(OH)_2$ has a relatively large band gap of 5.24 eV with GGA and 5.355 eV with LDA. . The gap goes down to 3.689 eV as Vanadium (V) replacement of 0 (no V) replacement goes up to 5. When all the phosphorus

(P) atoms are substituted by V atoms at a substitution level of 6, there was a slight increase in the band gap to 3.754 eV. It is evident in the graphs that the band gap is always in a direct gap which is located in the gamma direction of the Brillouin zone (see **Fig. 3(d)**). Moreover, it should be mentioned that the larger the concentration of Vanadium the flatter in the band structure calculations are the valence bands around the Fermi level. The flattening could also be a possible indication of interesting electrical and thermal transport properties, as flattened bands are an indication that there is a low dependence of energy on momentum and hence of large density of states.

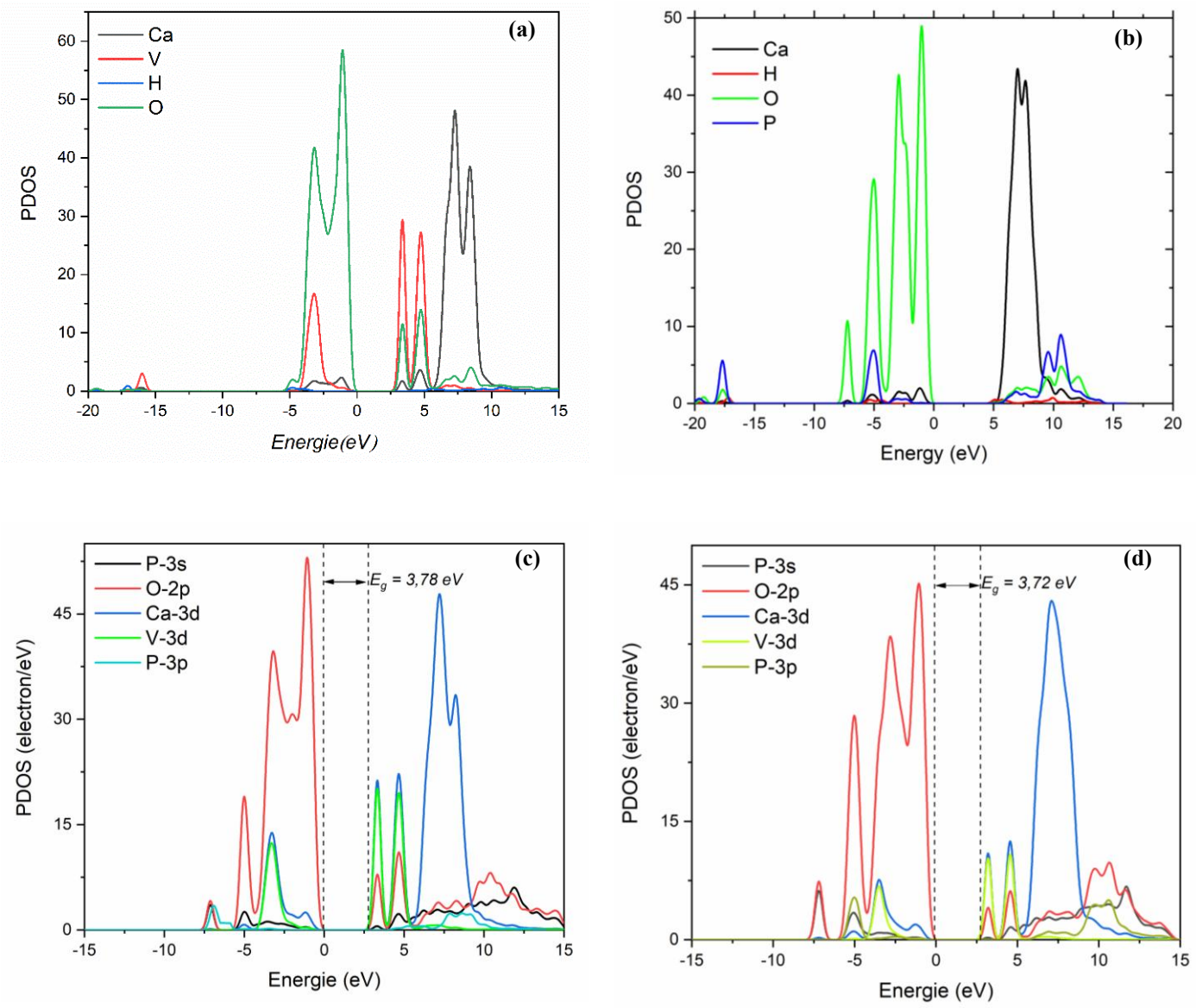

Fig. 4: (a)-(d) projected density of states of $Ca_{10}(PO_4)_x(VO_4)_{(6-x)}OH_2$ materials calculated by GGA for x=0, 2, 4 and 6 respectively

The flat bands observed may also be attributed to strong interactions between electrons within the material. This causes the electrons to become more localized, leading their behaviour to deviate from the independent particle model typically assumed in basic band theory.

Fig. 4 and **5** present the projected density of states calculated using the Generalized Gradient Approximation (GGA) and the Local Density Approximation (LDA), respectively. The figures reveal a notable similarity in the electron population patterns. However, the conduction states are slightly more populated in the GGA calculations compared to the LDA, particularly for the 3d states of Vanadium in the $Ca_{10}(VO_4)_6OH_2$ material, as shown in **Fig. 4 (a)** and **5 (a)**, This indicates that the contribution of different atomic orbitals to the material's conduction is greater in the GGA approximation. This difference arises mainly from how each approximation treats the electrons within the solid. Nevertheless, both approximations demonstrate that the incorporation of Vanadium into the Hydroxyapatite (HAP) structure will create accessible states within the band gap.

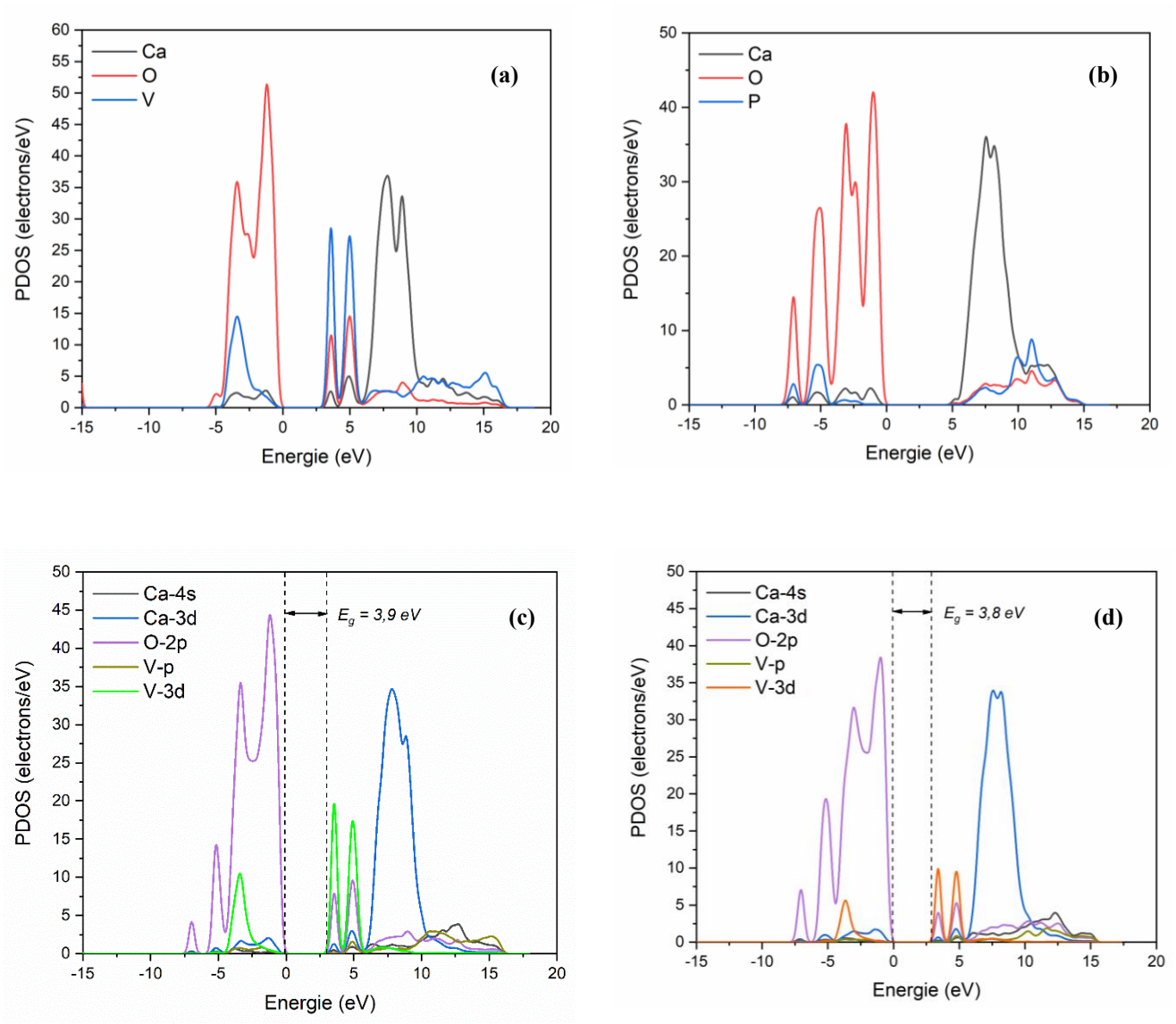

Fig. 5: (a)-(d) projected density of states of $Ca_{10}(PO_4)_x(VO_4)_{(6-x)}(OH)_2$ materials calculated by GGA for x=0, 2, 4 and 6 respectively.

The band structure and density of states were calculated, shown in **Fig. 5**, using Density Functional Theory (DFT) to gain a deeper understanding of how Vanadium (V) substitution affects the electronic properties of hydroxyapatite (HAP). In all figures presented, the valence band maximum of HAP is set at 0 eV. The obtained PBE band gap of pure HAP is 5.335 eV (GGA), and this correlates to the results obtained in literature [25,26].

According to the band structure analysis, as Vanadium (V) replaces Phosphorus (P) in hydroxyapatite the gap is. lower than that of pure HAP. To better explain how various atoms affect the electronic structure, we performed density of state (DOS) and projected density of state (PDOS) analyses. In pure hydroxyapatite, the Oxygen 2p orbitals make the largest contribution to the valence band, and the conductivity of the material is. primarily supplied by the 3d electrons of calcium, with a minor amount of the P-2p electrons.

When all the P atoms in the structure $Ca_{10}(VO_4)_6OH_2$ were substituted by V, we saw the density of states in the structure increased. the conduction band, and the band gap narrows. Here, the conductivity comes about due to the 3d electrons of both. calcium and vanadium. When comparing the PDOS of pure HAP (**Fig. 4(b)** and **5(b)**) with that of Vanadium-substituted HAP, the introduction of new energy states at the top of the valence band was noted. These new states result from the interaction between the 2p states of oxygen and the 3d energy states of the substituted Vanadium, as illustrated in **Fig. 4(c)** and **4(d)**. This interaction is the reason for the observed decrease in the band gap.

4. Conclusion

In this study, a geometrical optimization of the vanadium-substituted hydroxyapatite (NPs-HAP/VAP) structure using density functional theory (DFT) was performed. The optimized structures were then cleaved and sliced into slabs along the (001) direction to investigate the adsorption of RR141 dye molecules. The findings indicate that the dye adsorbs spontaneously onto the (001) surface of this material. However, the quality of adsorption and the preferred adsorption sites for the two dye molecules vary based on the amount of vanadium substitution. The electronic properties were also examined using the CASTEP module. This investigation focused on how the level of dopant affects the electronic structure of hydroxyapatite. The results demonstrate that the material retains its semiconducting nature even with an increase in vanadium content within the pure HAP structure. Nevertheless, the electronic properties specifically the energy gap, density of states (DOS), and partial density of states (PDOS) are influenced by the substitution of vanadium in the initial structure.

References

[1] X. Zhao, Y. Zhang, Y. Guo, H. Yuan, J. Guan, Q. Huang, Preparation of magnetic hydroxyapatite whisker and its adsorption capacity to cadmium ion, Materials Today Communications 38 (2024) 108116. https://doi.org/10.1016/j.mtcomm.2024.108116.

[2] N.M. Basfer, S.F. Mansour, M.K. Ahmed, Physicochemical properties of hydroxyapatite modified with vanadium ions for degradation of methylene blue, Journal of Molecular Structure 1240 (2021) 130562. https://doi.org/10.1016/j.molstruc.2021.130562.

[3] F.Z. Chajri, M. Bensemlali, B. Hatimi, M. Joudi, A. Aarfane, M. Monkade, L. El Gaini, M. Bakasse, H. Nasrellah, Sustainable synthesis of vanadate/fluorapatite nano-crystallites from solid waste for enhanced photocatalysis and pollution removal, Matériaux & Techniques 111 (2023) 505. https://doi.org/10.1051/mattech/2024007.

[4] I.L. Balasooriya, J. Chen, S.M. Korale Gedara, Y. Han, M.N. Wickramaratne, Applications of Nano Hydroxyapatite as Adsorbents: A Review, Nanomaterials (Basel) 12 (2022) 2324. https://doi.org/10.3390/nano12142324.

[5] A. Biedrzycka, E. Skwarek, U.M. Hanna, Hydroxyapatite with magnetic core: Synthesis methods, properties, adsorption and medical applications, Adv Colloid Interface Sci 291 (2021) 102401. https://doi.org/10.1016/j.cis.2021.102401.

[6] S. Tizazu, G. Tesfaye, A. Wang, A. Guadie, B. Andualem, Microbial diversity, transformation and toxicity of azo dye biodegradation using thermo-alkaliphilic microbial consortia, Heliyon 9 (2023) e16857. https://doi.org/10.1016/j.heliyon.2023.e16857.

[7] S. Vinitnantharat, W. Chartthe, A. Pinisakul, Toxicity of reactive red 141 and basic red 14 to algae and waterfleas, Water Sci Technol 58 (2008) 1193–1198. https://doi.org/10.2166/wst.2008.476.

[8] Z. Bonyadi, Z. Fouladi, A. Robatjazi, M. Zahmatkesh Anbarani, Reactive red-141 removal from synthetic solutions by γ-Al2O3 nanoparticles: process modeling, kinetic, and isotherm studies, Appl Water Sci 13 (2023) 52. https://doi.org/10.1007/s13201-022-01854-6.

[9] H. Behloul, H. Ferkous, N. Bougdah, S. Djellali, M. Alam, C. Djilani, A. Sedik, D. Lerari, B.-H. Jeon, Y. Benguerba, New insights on the adsorption of CI-Reactive Red 141 dye using activated carbon prepared from the ZnCl2-treated waste cotton fibers: Statistical physics, DFT, COSMO-RS, and AIM studies, Journal of Molecular Liquids 364 (2022) 119956. https://doi.org/10.1016/j.molliq.2022.119956.

[10] H. Hafdi, M. Joudi, J. Mouldar, B. Hatimi, H. Nasrellah, M.A. El Mhammedi, M. Bakasse, Design of a new low cost natural phosphate doped by nickel oxide nanoparticles for capacitive adsorption of reactive red 141 azo dye, Environ Res 184 (2020) 109322. https://doi.org/10.1016/j.envres.2020.109322.

[11] M.E. Belghiti, J. Mouldar, M. Bakasse, Computational Study of the Interaction between Azo Dye (Rr141) and Hematite A-Fe2o3(111) Surface: Density Functional Theory and Molecular Dynamics Simulation, (2023). https://doi.org/10.2139/ssrn.4511089.

[12] K. Oueslati, A. Naifar, K.S. Al-mugren, F. Aouaini, A.B. Lamine, Theoretical assessment of the adsorption mechanism of Reactive Red 141 on metal hydroxide: water remediation via statistical physics modelling, Surfaces and Interfaces 51 (2024) 104631. https://doi.org/10.1016/j.surfin.2024.104631.

[13] M.M.S. Ali, D.M. Imam, Y.A. El-Nadi, Vanadium(V) removal and recovery by adsorption onto modified activated carbon derived from natural hydroxyapatite, J IRAN CHEM SOC 18 (2021) 2771–2784. https://doi.org/10.1007/s13738-021-02227-7.

[14] S. Petit, T. Gode, C. Thomas, S. Dzwigaj, Y. Millot, D. Brouri, J.-M. Krafft, G. Rousse, C. Laberty-Robert, G. Costentin, Incorporation of vanadium into the framework of hydroxyapatites: importance of the vanadium content

and pH conditions during the precipitation step, Physical Chemistry Chemical Physics 19 (2017) 9630–9640. https://doi.org/10.1039/C6CP08782E.

[15] A New One-Step Synthesis of Nanostructured Calcium Vanadate/Phosphate Apatite for Vanadate and Phosphorus Waste Valorisation: Characterization and Band Gap Determination, Biointerface Res Appl Chem 14 (2024) 40. https://doi.org/10.33263/BRIAC142.040.

[16] F.Z. Chajri, M. Bensemlali, B. Hatimi, M. Joudi, A. Aarfane, M. Monkade, L. El Gaini, M. Bakasse, H. Nasrellah, Sustainable synthesis of vanadate/fluorapatite nano-crystallites from solid waste for enhanced photocatalysis and pollution removal, Matériaux & Techniques 111 (2023) 505. https://doi.org/10.1051/mattech/2024007.

[17] F.Z. Chajri, M. Bensemlali, B. Hatimi, A. Sanad, M. Joudi, A. Aarfane, M. Siniti, M. Bakasse, A. Baraket, H. Nasrellah, Study on Wastewater Treatment in the Textile Industry by Adsorption of Reactive Red 141 Dye Using a Phosphogypsum/Vanadium Composite Developed from Phosphate Industry Waste., Ecological Engineering & Environmental Technology (EEET) 25 (2024). http://www.ecoeet.com/pdf-187922-110101?filename=Study (accessed December 3, 2024).

[18] M. Corno, C. Busco, V. Bolis, S. Tosoni, P. Ugliengo, Water Adsorption on the Stoichiometric (001) and (010) Surfaces of Hydroxyapatite: A Periodic B3LYP Study, Langmuir 25 (2009) 2188–2198. https://doi.org/10.1021/la803253k.

[19] A.A. El Hassani, K. Tanji, I. El Mrabet, Y. Fahoul, A. El Gaidoumi, A.T. Benjelloun, M. Sfaira, H. Zaitan, A. Kherbeche, A combined molecular dynamics simulation, DFT calculations, and experimental study of the adsorption of Rhodamine B dye on kaolinite and hydroxyapatite in aqueous solutions, Surfaces and Interfaces 36 (2023) 102647. https://doi.org/10.1016/j.surfin.2023.102647.

[20] F. Chiatti, M. Corno, P. Ugliengo, Stability of the Dipolar (001) Surface of Hydroxyapatite, J. Phys. Chem. C 116 (2012) 6108–6114. https://doi.org/10.1021/jp212595d.

[21] M.-H. Ri, Y.-M. Jang, U.-S. Ri, C.-J. Yu, K.-I. Kim, S.-U. Kim, Ab initio Investigation of Adsorption Characteristics of Bisphosphonates on Hydroxyapatite (001) Surface, J Mater Sci 53 (2018) 4252–4261. https://doi.org/10.1007/s10853-017-1880-1.

[22] J. Song, N. Cui, X. Mao, Q. Huang, E.-S. Lee, H. Jiang, Sorption Studies of Tetracycline Antibiotics on Hydroxyapatite (001) Surface—A First-Principles Insight, Materials 15 (2022) 797. https://doi.org/10.3390/ma15030797.

[23] M. Corno, R. Orlando, B. Civalleri, P. Ugliengo, Periodic B3LYP study of hydroxyapatite (001) surface modelled by thin layer slabs, European Journal of Mineralogy 19 (2007) 757–767. https://doi.org/10.1127/0935-1221/2007/0019-1764.

[24] C. Wu, Y. Wang, Y. Hou, X. Li, Z. Peng, Q. Du, M. Ni, K. Jiao, Reconstruction and optimization of LSCF cathode microstructure based on Kinetic Monte Carlo method and Lattice Boltzmann method, Chemical Engineering Journal 436 (2022) 132144. https://doi.org/10.1016/j.cej.2021.132144.

[25] K. Matsunaga, A. Kuwabara, First-principles study of vacancy formation in hydroxyapatite, Phys. Rev. B 75 (2007) 014102. https://doi.org/10.1103/PhysRevB.75.014102.

[26] V. Bystrov, E. Paramonova, L. Avakyan, J. Coutinho, N. Bulina, Simulation and Computer Study of Structures and Physical Properties of Hydroxyapatite with Various Defects, Nanomaterials 11 (2021) 2752. https://doi.org/10.3390/nano11102752.